bioRxiv preprint doi: https://doi.org/10.1101/2022.10.04.510779; this version posted November 24, 2022. The copyright holder for this preprint (which was not certified by peer review) is the author/funder, who has granted bioRxiv a license to display the preprint in perpetuity. It is made available under aCC-BY 4.0 International license.

No Brain Signature of Prediction Error to Unattended Visual Stimuli Despite Early Brain Encoding of the Stimuli

Alie G. Male[1,2] and Robert P. O'Shea[1,3]

1 Discipline of Psychology, College of Science, Health, Engineering and Education, Murdoch University, Perth, Australia

2 Department of Psychiatry and Human Behavior, School of Medicine, University of California, Irvine, USA

3 Wilhelm Wundt Institute for Psychology, University of Leipzig, Leipzig, Germany

Corresponding author

Please address all correspondence concerning this article to Alie Male, Department of Psychiatry and Human Behavior, School of Medicine, University of California, Irvine, USA

E-mail: alie.male@live.com

bioRxiv preprint doi: https://doi.org/10.1101/2022.10.04.510779; this version posted November 24, 2022. The copyright holder for this preprint (which was not certified by peer review) is the author/funder, who has granted bioRxiv a license to display the preprint in perpetuity. It is made available under aCC-BY 4.0 International license.

Abstract

Prediction error is a basic component of predictive-coding theory of brain processing. According to the theory, each stage of brain processing of sensory information generates a model of the current sensory input; subsequent input is compared against the model and only if there is a mismatch, a prediction error, is further processing performed. Recently, Smout et al. [1] found that a signature of prediction error, the visual (v) mismatch negativity (MMN), for a fundamental property of visual input—its orientation—was absent without attention on the stimuli. This is remarkable because the weight of evidence for MMNs from audition and vision is that they occur without attention. To resolve this discrepancy, we conducted an experiment addressing two alternative explanations for Smout et al.'s finding: that it was from a lack of reproducibility or that participants' visual systems did not encode the stimuli when attention was on something else.

We conducted a similar experiment to Smout et al.'s. We showed 21 participants sequences of identically oriented Gabor patches, standards, and, unpredictably, otherwise identical, Gabor patches differing in orientation by ±15°, ±30°, and ±60°, deviants. To test whether participants encoded the orientation of the standards, we varied the numbers of standards preceding a deviant, allowing us to search for a decrease in activity with the number of repetitions of standards—repetition suppression. We diverted participants' attention from the oriented stimuli with a central, letter-detection task.

We reproduced Smout et al.'s finding of no vMMN without attention, strengthening their finding. We also found that our participants showed

bioRxiv preprint doi: https://doi.org/10.1101/2022.10.04.510779; this version posted November 24, 2022. The copyright holder for this preprint (which was not certified by peer review) is the author/funder, who has granted bioRxiv a license to display the preprint in perpetuity. It is made available under aCC-BY 4.0 International license.

repetition suppression: they did encode the stimuli pre-attentively. We also found early processing of deviants. We discuss whether this earlier processing of deviants may be why no further processing, in the vMMN time window, occurs.

Keywords: predictive-coding theory, mismatch negativity, MMN, visual mismatch negativity, vMMN, orientation, EEG, ERP, reproducibility, repetition suppression, deviant-related activity, deviant-related positivity,

bioRxiv preprint doi: https://doi.org/10.1101/2022.10.04.510779; this version posted November 24, 2022. The copyright holder for this preprint (which was not certified by peer review) is the author/funder, who has granted bioRxiv a license to display the preprint in perpetuity. It is made available under aCC-BY 4.0 International license.

No Brain Signature of Prediction Error to Unattended Visual Stimuli Despite Early Brain Encoding of the Stimuli

Our senses are flooded by information. For example, the four million cones of the human retina encode a staggering 101,200,000 bits of information at any instant if their responses to light were binary (which they are not) [2]. Still, we do not experience a flood—only a stream—of information to which we pay attention or of which we become conscious [3]. What we see does not require such an impossible burden of encoding because it is highly redundant, allowing prediction of the state of one photoreceptor at any instant from its state the instant before and from the state of its neighbors. This seminal idea developed into predictive-coding theory, first of the retina [4] and then of the brain's hierarchical sensory systems [5, 6].

Predictive coding theory is a leading theory of how the brain deals with sensory input [7]. It is that the brain uses recent, past, bottom-up, sensory information, along with top-down information (such as prior probabilities, expectations, and attention) to generate predictive models of sensory input at various levels of the sensory pathway. If future inputs match the prediction, no further processing is required. If they do not match—a so-called prediction error—further processing occurs to update the model.

We studied the visual mismatch negativity (vMMN) as our signature of prediction error [8]. The vMMN is an event-related potential (ERP) from electroencephalography. Stefanics et al. [8] have reviewed its hundreds of studies: It is evoked by an unpredicted change in what we see. It occurs when a rare, unpredicted, deviant, visual stimulus occurs after a sequence of identical,

bioRxiv preprint doi: https://doi.org/10.1101/2022.10.04.510779; this version posted November 24, 2022. The copyright holder for this preprint (which was not certified by peer review) is the author/funder, who has granted bioRxiv a license to display the preprint in perpetuity. It is made available under aCC-BY 4.0 International license.

standard, visual stimuli in a so-called oddball sequence. It is greater ERP negativity from parieto-occipital (PO) recording sites for deviants than for standards, occurring between 150 ms and 300 ms after the onset of the deviant. It occurs without adaptation, showing the genuine vMMN [9]. It is supposed to occur without attention on the deviant property of the stimuli.

Recently however, Smout et al. [1] found no ERP evidence of the genuine vMMN without attention to unexpected changes in orientation. In their attended condition, they showed each participant displays consisting of an annular Gabor patch with a central black spot. They asked the participant to look only at the spot but to pay attention to the bars of the Gabor and to press a button on rare occasions when the bars' spatial frequency increased. In their ignored condition, the same participant viewed the same displays but paid attention to the spot and pressed a button on rare occasions when its contrast decreased. The difficulty of the two tasks was equated for each participant in prior psychophysical testing.

Smout et al.'s stimuli of interest were the Gabor annuli. Participants viewed different-length sequences of displays of identical annuli—standards—followed by an otherwise identical annulus but with bars differing in orientation by ±20°, ±40°, ±60°, or ±80°—a deviant. On the next display, the deviant annulus was repeated, commencing a new sequence for which it now served as the standard—the so-called roving-standard paradigm [10]. To measure the genuine vMMN, Smout et al. also showed control sequences in which all possible orientations occurred in random order, from which no expectation could be established, yet which had the same overall frequency of

bioRxiv preprint doi: https://doi.org/10.1101/2022.10.04.510779; this version posted November 24, 2022. The copyright holder for this preprint (which was not certified by peer review) is the author/funder, who has granted bioRxiv a license to display the preprint in perpetuity. It is made available under aCC-BY 4.0 International license.

stimuli identical to deviants, equating adaptation—the equiprobable control [11].

Smout et al. found a genuine vMMN from PO electrodes to unexpected changes in the orientation of the bars in the attended condition (between about 170 ms to about 300 ms), but not in the ignored condition (their Figure S1B). They did find genuine, deviant-related responses in the ignored condition: a negativity from about 330–430 ms from a midline central electrode (Cz) and from about 300–470 ms from a midline frontal electrode (Fz). But these are too late to be considered vMMNs, or any sort of prediction error from such an early brain-processing feature of visual input as orientation [12].

Smout et al. confined their remaining clever analyses to their attended condition to answer questions about the timing and orientation tuning of prediction error. But their failure to find a genuine vMMN without attention was wildly unexpected. Smout et al. did not discuss it except to cite one study for a similar finding in the auditory modality [13]. To resolve this discrepancy, we conducted an experiment addressing two alternative explanations for Smout et al.'s finding: that it was from a lack of reproducibility or that participants' visual systems did not encode the stimuli when attention was on something else.

We made some changes to improve our study's ability to detect the genuine vMMN and to enhance its design. Smout et al.'s stimuli were Gabor annuli with an outer diameter of 11° diameter and an inner diameter of 0.83°; their inner grey patch interrupted the central bars over a region of about the size of the human foveola to which about 20% of the processing of the visual

bioRxiv preprint doi: https://doi.org/10.1101/2022.10.04.510779; this version posted November 24, 2022. The copyright holder for this preprint (which was not certified by peer review) is the author/funder, who has granted bioRxiv a license to display the preprint in perpetuity. It is made available under aCC-BY 4.0 International license.

system is devoted [14]. To improve our chances of finding a vMMN, our Gabor patches were double the size of Smout et al.'s outer diameter size, and our central bars were continuous except for a very small area occupied by the lines of small task-relevant fixation letters. We also omitted an attended condition, eliminating any possible confound in Smout et al.'s design from participants' moving their eyes to the bars [15], thus bringing them onto central vision. We also analyzed clusters of electrodes around the single electrodes Smout et al. reported. This was to avoid issues related to variability in placement of single electrodes [16].

To look for evidence that participants encoded the orientation of the Gabor patches, we searched for repetition suppression: attenuated brain activity to repeated stimuli [17]. For Gabor patches similar to those used by Smout et al. and by us, this attenuation appears in various components of ERPs, as late as the P2 [17] and as early as the P1 at occipital-parietal electrodes [18].

We found no genuine vMMN to ignored orientation deviants despite showing that participants encoded the orientated stimuli.

Results

Participants looked at a central, desynchronized stream of letters and pressed a key whenever an X appeared (Figure 1A-B). Desynchronized from the letter stream, Gabor patches appeared with, in experimental blocks, occasional changes in orientation after varying numbers of repetitions of the same orientation and, in control blocks, randomly selected orientations on each trial (Figure 1C-D).

bioRxiv preprint doi: https://doi.org/10.1101/2022.10.04.510779; this version posted November 24, 2022. The copyright holder for this preprint (which was not certified by peer review) is the author/funder, who has granted bioRxiv a license to display the preprint in perpetuity. It is made available under aCC-BY 4.0 International license.

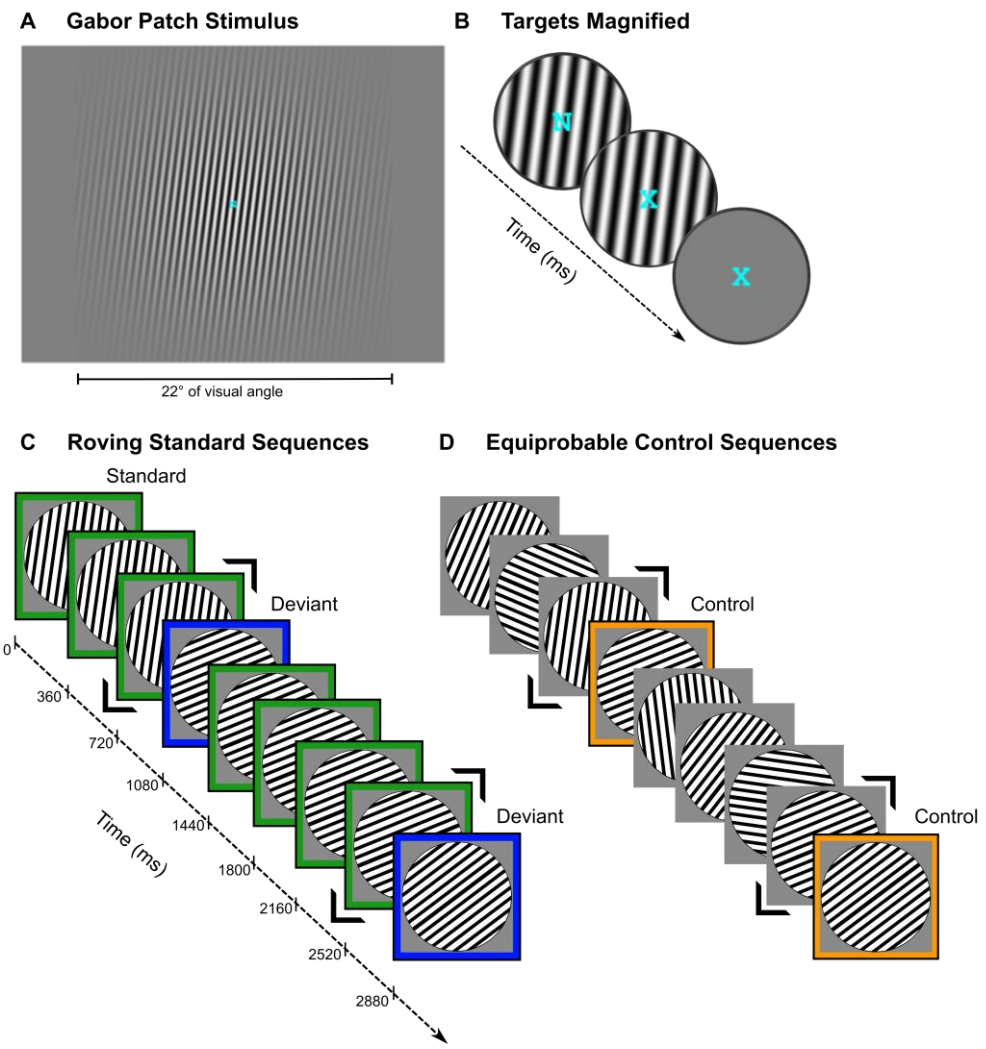

Figure 1. **Experimental Paradigm. A. Screenshots from the experiment of a Gabor patch** tilted 8° clockwise from vertical (0°), with a superimposed fixation letter. **B. Magnified views of a sequence of target letters** superimposed on the Gabor patch (first two images) or on the gray screen during the inter-stimulus interval (ISI). The participants' task was to press a key whenever an X appeared. Each letter was shown for 600 ms. **C. Illustration of roving standard sequences** in which the first few trials of one sequence is 8°... 8°... 8°... *68*° (i.e., +60° orientation deviant for the first sequence) then ...68°... 68°... 68°... 68°... *53*°... (i.e., -15° orientation deviant for the second sequence). Standards are outlined in green; deviants are outlined in blue. The stimulus preceding a deviant is framed with two black chevrons. **D. Illustration of matching equiprobable controls** in which we replaced standard stimuli—except for the ones immediately preceding a deviant from the corresponding roving standard sequence—with Gabor patches whose orientation was randomly chosen among the 12 possible orientations. All orientations appeared equally (8.3%) often. The stimulus in the sequence (also

bioRxiv preprint doi: https://doi.org/10.1101/2022.10.04.510779; this version posted November 24, 2022. The copyright holder for this preprint (which was not certified by peer review) is the author/funder, who has granted bioRxiv a license to display the preprint in perpetuity. It is made available under aCC-BY 4.0 International license.

framed with two black chevrons) preceding the one that would have been the deviant in the corresponding roving standard sequence had an identical orientation to that from the corresponding roving standard sequence. The control (outlined in orange) also had the same orientation as that of the deviant from the corresponding roving standard sequence. Gabor patch onset is indicated on the timeline. Stimuli appeared for 80 ms, followed by a grey interstimulus interval (ISI) screen for 280 ms (not shown).

Did our Participants Attend to the Letter-Detection Task, Thereby Ignoring the Gabor Patches?

We checked whether our participants attended to the central, letter-detection task, thereby ignoring the Gabor patches. The mean hit rate for detecting the target X in the central letter stream was 98.2% and the mean false alarm rate was <0.01%, showing that participants paid attention to the task and did very well on it. There were no significant differences in performance of the task on oddball and control blocks (details of analyses in supplementary materials: S1).

Did we Find a vMMN to Unpredicted Orientation Changes?

We did not find a genuine vMMN to unpredicted ignored orientation changes. There is no hint of any genuine negativity in the vMMN time range to any unpredicted orientation changes from any electrode cluster (we give details of our analyses, including Bayesian statistical tests, in Table S1). We show the ERPs and the difference waves in Figure 2, formatted similarly to those of Smout et al.'s. For simplicity, we give our results only for the ±60° orientation change, 10° larger than the average orientation change Smout et al. used. We give the ERPs and the difference waves for our other two orientation changes in Figures S1 and S2. Those difference waves also show no evidence of the

bioRxiv preprint doi: https://doi.org/10.1101/2022.10.04.510779; this version posted November 24, 2022. The copyright holder for this preprint (which was not certified by peer review) is the author/funder, who has granted bioRxiv a license to display the preprint in perpetuity. It is made available under aCC-BY 4.0 International license.

vMMN. That is, we replicated Smout et al.'s unexpected failure to find a vMMN, strengthening their finding (details in supplementary materials: S2.1). To take another approach to describing our data, we used temporal principal component analysis (PCA; [19]). We found no component that was consistent with a vMMN.

We also found genuine deviant-related activity outside the vMMN time range: a positivity we call the deviant-related positivity (DRP) from PO electrodes about 90 ms after onset of unpredicted orientation changes. PCA showed that this positivity was from the P1. Figure 3 illustrates these findings (details of analyses in supplementary materials: 2.2).

Smout et al. showed no sign of this early component in their ignored condition. This could be because they obscured the bars of the Gabor patch from central vision by their 0.83°-diameter grey patch, unlike in our study in which the bars crossed central vision.

bioRxiv preprint doi: https://doi.org/10.1101/2022.10.04.510779; this version posted November 24, 2022. The copyright holder for this preprint (which was not certified by peer review) is the author/funder, who has granted bioRxiv a license to display the preprint in perpetuity. It is made available under aCC-BY 4.0 International license.

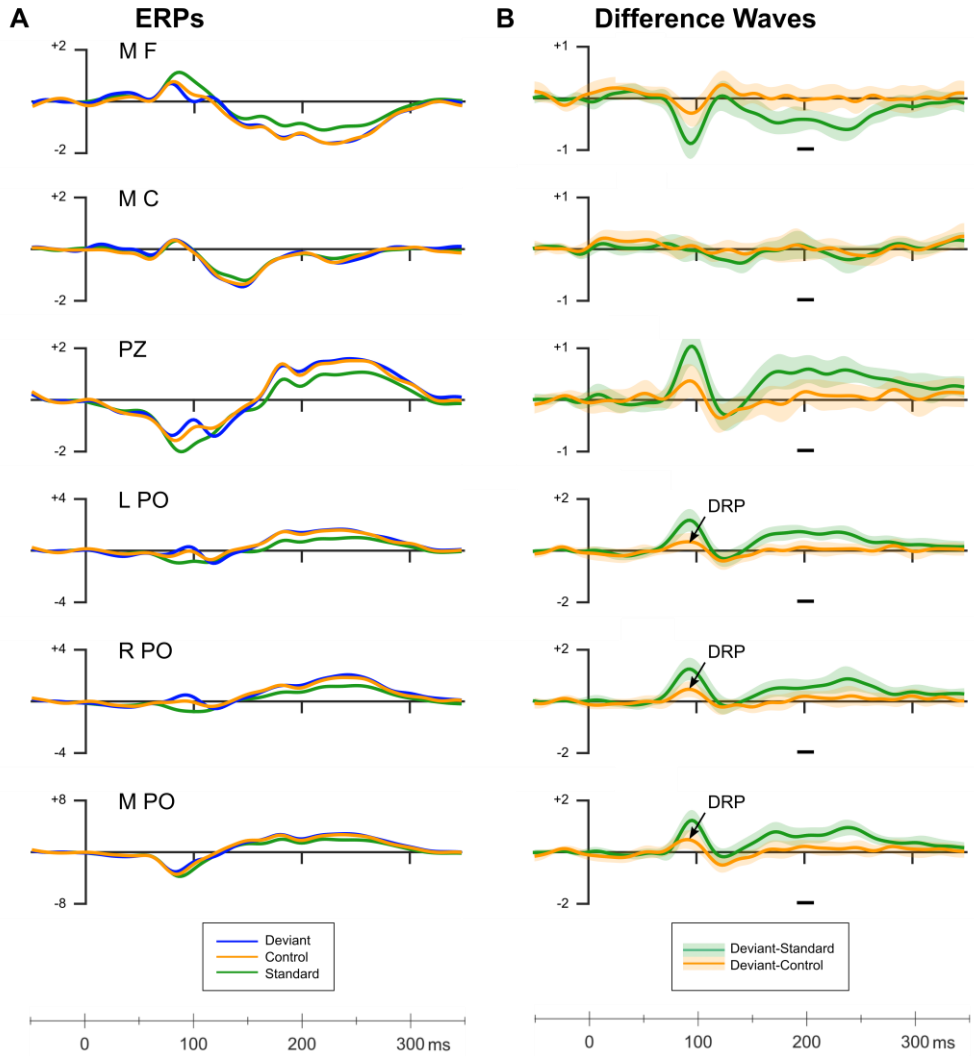

Figure 2. A. **Grand average ERPs from various electrode clusters** around the electrodes Smout et al. reported. B. **Difference waves for classic (60-degree deviant minus standard) and genuine (60-degree deviant minus 60-degree control) deviant-related activity**. The arrowed components show the only genuine deviant-related activity (DRP). Horizontal grey bars illustrate the time window in which Kimura and Takeda (2015) found the largest deviant-minus-control difference (i.e., genuine vMMN) for 32.7° orientation deviants. Amplitudes from this time window were analyzed using Bayesian replication tests (results in Table S1). The lighter colors surrounding the difference waves give ± 1 standard error of the mean.

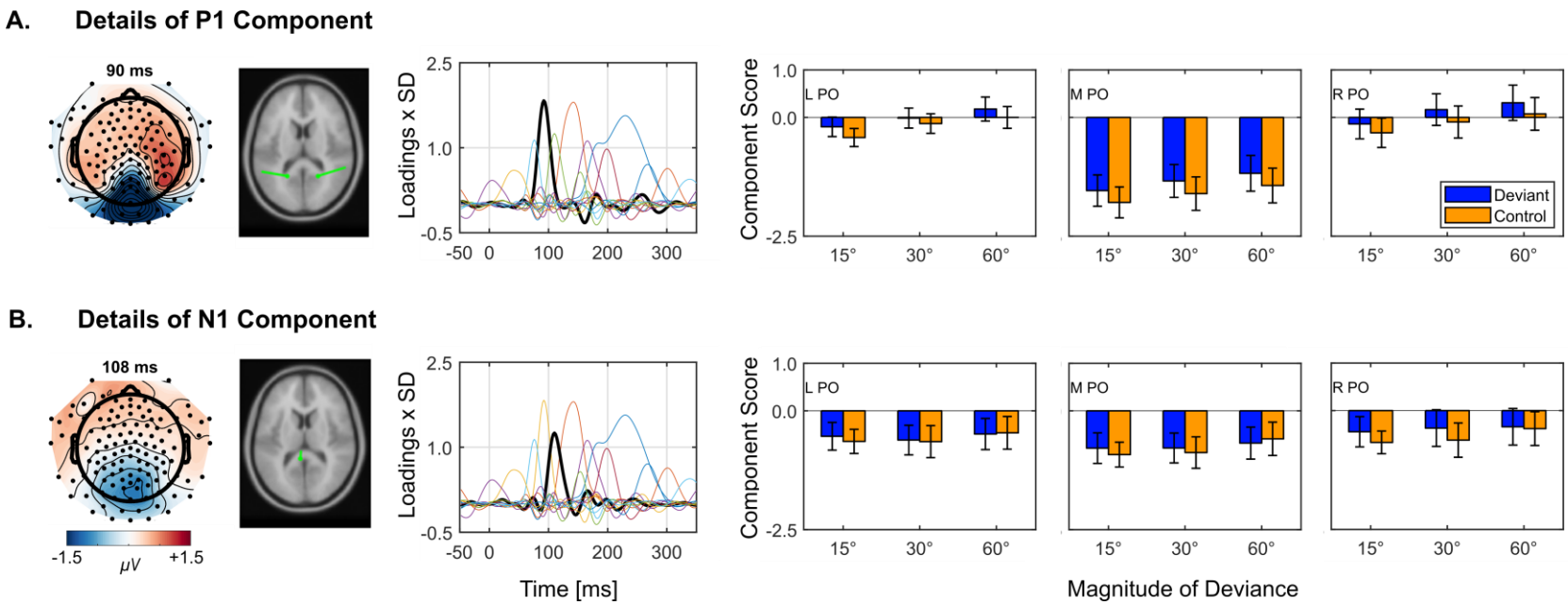

Figure 3. **PCA component details for the P1 and N1 components of genuine deviant-related activity. A. PCA details of the P1. B. PCA details of the N1**. The topographic maps in leftmost column show the combined activity from deviant and control trials at peak latency of the P1 (top) and N1 (bottom). In the second column, we show the results of our dipole analysis of each component. Dipole analysis shows that the pronounced negativity at the M PO reflects the combined negative pole of both P1 components converging within close proximity. In the third column, we show the component loadings (scaled by SD) (thick black line) relative to all other components (thin multi-colored lines). This illustrates the component's contribution to the overall evoked activity recorded from the scalp. In columns four to six, we show the scores for deviant (orange) and control (purple) trials for each magnitude of deviance (15°, 30°, 60°) at the left (L), midline (M), and right parieto-occipital (PO) region. Error bars depict ±1 standard error. Statistical analyses show that the deviant-related positivity at PO regions in Figure 2 are statistically significant for deviant-minus-control positivity for the P1 only (details in supplementary materials: S2.1).

bioRxiv preprint doi: https://doi.org/10.1101/2022.10.04.510779; this version posted November 24, 2022. The copyright holder for this preprint (which was not certified by peer review) is the author/funder, who has granted bioRxiv a license to display the preprint in perpetuity. It is made available under aCC-BY 4.0 International license.

Did we Find Repetition Suppression?

We did find repetition suppression (as did Smout et al. in their attended condition). To search for it we used PCA to identify plausible components. We found two components showing repetition suppression—the N1 and P2, most clearly for the P2 (Figure 4). We show the N1 in Figure S3. Figure 4 shows that the PCA P2 scores became significantly less positive with increasing sequential position (i.e., repeated presentations) of standards (green points and regression lines). The P2 scores to random changes (black points and regression lines) became slightly more positive with sequential position, but these are not significant. The results from the standard stimuli show clearly that our participants encoded them, so the absence of a vMMN cannot have been from lack of encoding.

bioRxiv preprint doi: https://doi.org/10.1101/2022.10.04.510779; this version posted November 24, 2022. The copyright holder for this preprint (which was not certified by peer review) is the author/funder, who has granted bioRxiv a license to display the preprint in perpetuity. It is made available under aCC-BY 4.0 International license.

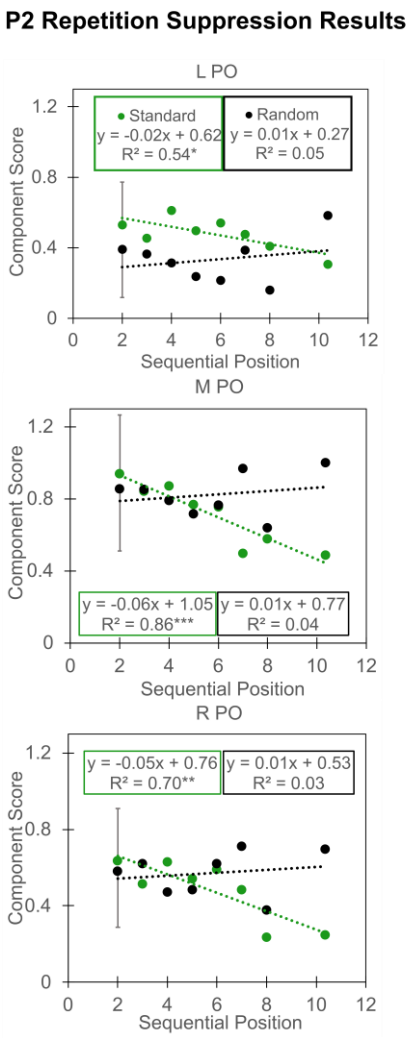

Figure 4. **P2 repetition suppression results.** P2 PCA scores are shown separately for the left (L), midline (M), and right (R) parietal-occipital (PO) regions of interest (ROI). Regression equations show the dotted lines in the data for standard and random stimuli. Asterisks denote the linear regression significance: **p*<.05, ***p*<.01, *** *p*<.001. Error bars show 1 standard error (SE) calculated as the mean SE for all sequential positions. SE bars appear only on the second sequential position. We show +1 SE for standard and –1 SE for random stimuli.

Discussion

We have shown that even though participants encoded stimuli, they failed to show a genuine vMMN to unexpected orientation changes when they attended to a central task. Absence of the vMMN is consistent with five

bioRxiv preprint doi: https://doi.org/10.1101/2022.10.04.510779; this version posted November 24, 2022. The copyright holder for this preprint (which was not certified by peer review) is the author/funder, who has granted bioRxiv a license to display the preprint in perpetuity. It is made available under aCC-BY 4.0 International license.

experiments including ours [1, 15, 20, 21], but inconsistent with four [11, 22-24]. There are at least three possible explanations for this empirical dilemma:

1. There really is no genuine vMMN to unexpected, unattended orientation changes and the four out of nine studies that reported it are examples of publication bias or methodological errors.
2. There is a genuine vMMN to unexpected, unattended orientation changes and the five studies that failed to find it suffered from some yet-to-be-determined methodological differences or problems.
3. The vMMN is not the appropriate sign of prediction error for isolated and well controlled changes in low-level features of visual input—features that are easily processed in V1.

1. No Genuine vMMN to Unexpected Orientation Changes?

Although a 44% hit rate for finding a genuine vMMN is something to take notice of, it is possible there are other negative studies that never made it into print. The vMMN literature does indeed show signs of publication bias. For example, of the 22 orientation vMMN published studies, including those only on the classic vMMN, we are aware of only four reporting no vMMN for a hit rate of 82%. All but one [15] also reported a different condition or experiment in which a vMMN was found, suggesting that vMMN experiments in which all conditions failed to show a vMMN are either not submitted for publication or submitted and rejected. We are aware from a personal communication of at least one such unpublished orientation experiment; there may be more. Such a bias would make it difficult to identify the experimental

bioRxiv preprint doi: https://doi.org/10.1101/2022.10.04.510779; this version posted November 24, 2022. The copyright holder for this preprint (which was not certified by peer review) is the author/funder, who has granted bioRxiv a license to display the preprint in perpetuity. It is made available under aCC-BY 4.0 International license.

parameters required to resolve whether the genuine vMMN to orientation changes occurs without attention.

2. Methodological Differences or Problems?

We considered whether our experimental parameters were responsible for our results and decided not. Human observers can discriminate orientation differences between gratings of about 0.4° [25], so there is no question that even our smallest orientation difference of 15° is large enough to be perceived. Others have shown genuine vMMNs for other unattended, more complex deviants with presentation times as short as 17 ms [26], much shorter than our 80 ms. And others have shown genuine vMMNs with ISIs as short as 210 ms [27], shorter than our 280 ms. It seems unlikely our choices of orientation change, presentation time, and ISI were responsible for our failure to find a genuine vMMN.

In a review of the literature, we noted that researchers generally failed to isolate individual low-level features, such as orientation, from other, confounding factors including eye movements that are capable of changing simple orientation changes into more complex visual changes [15]. Even Smout et al.'s study suffers from this, with very careful control of fixation in their ignored condition (the participants' task was to detect contrast changes in a small central spot, requiring them to look at it) but not in their attended condition (the participants' task was to detect spatial-frequency changes in the bars of the oriented stimuli, 0.42° away from the fixation spot). Male et al. [15] showed evidence that participants' eyes did stray away from central fixation

bioRxiv preprint doi: https://doi.org/10.1101/2022.10.04.510779; this version posted November 24, 2022. The copyright holder for this preprint (which was not certified by peer review) is the author/funder, who has granted bioRxiv a license to display the preprint in perpetuity. It is made available under aCC-BY 4.0 International license.

when the task-relevant information was away from fixation, despite instructions to keep fixation central.

3. The vMMN is not the Appropriate Sign of Prediction Error for Low-level Visual Features?

It is possible that unexpected changes in low-level features, such as orientation, are processed earlier than would normally be considered to fall into the time range of the vMMN. We found a genuine, deviant-related positivity at the P1, about 90 ms after onset of the Gabor patch. We have previously reported similar early deviant-related positivity [15] for orientation and for other basic stimulus features. Others have also reported early positivities for deviants, although these do not appear to have been considered as indicators of deviance detection [21, 28-33].

Alternatively, one could argue that we, like Smout et al. and others, did not find the genuine vMMN because prediction error generation in the visual system, unlike the auditory system, requires attention. This would, however, undermine one of the most frequently cited evolutionary purposes of prediction error; to monitor one's immediate surroundings pre-attentively. Smout et al. carefully navigated this obstacle, saying only that attention enhances the processing of unexpected changes in visual input. We also prefer to leave predictive-coding theory intact and point out that our finding of earlier processing of unexpected orientation changes suggests that no later processing, in the vMMN time range, is necessary.

bioRxiv preprint doi: https://doi.org/10.1101/2022.10.04.510779; this version posted November 24, 2022. The copyright holder for this preprint (which was not certified by peer review) is the author/funder, who has granted bioRxiv a license to display the preprint in perpetuity. It is made available under aCC-BY 4.0 International license.

We hope we have convinced you that the early positivity we found is a useful lead to understanding how the absence of a vMMN without attention could be reconciled with predictive coding theory.

Methods

We showed 21 [24 in Smout et al.] participants sequences of identically oriented Gabor patches (Figure 1A), standards, and, unpredictably, otherwise identical Gabor patches differing in orientation by ±15°, ±30°, and ±60° [±20°, ±40°, ±60°, or ±80° in Smout et al.], deviants (80 ms duration [100 ms], 280-ms [500 ms] ISI, 634 patches [415] per block; see Figure 1A). Participants looked at a central, desynchronized stream of letters and pressed a key whenever an X appeared (Figure 1B). Standard sequences ranged in length randomly from 3 to more than 11. For an equiprobable control, we presented the same stimuli, but in a random order (see Figure 1D).

Participants

Twenty-one self-declared healthy adults (8 males, 18 right-handed) with normal or corrected-to-normal vision participated in the experiment (statistical power = .88, based on Kimura and Takeda's [22] reported effect size for genuine vMMN at PO8: Cohen's $d = -0.73$). Mean age was 33 years with a range from 18 to 60 years. Most of the participants were undergraduate psychology students at Murdoch University. All participants provided their written informed consent and were free to withdraw from the experiment at any time. Participants received course credit or entry into a draw to win a $50 gift card in return for participation. The Human Research Ethics Committee at Murdoch University approved the experiment (permit 2015 208).

bioRxiv preprint doi: https://doi.org/10.1101/2022.10.04.510779; this version posted November 24, 2022. The copyright holder for this preprint (which was not certified by peer review) is the author/funder, who has granted bioRxiv a license to display the preprint in perpetuity. It is made available under aCC-BY 4.0 International license.

Apparatus

Participants sat in a light-attenuated chamber viewing a calibrated monitor (17-inch, color, cathode-ray-tube display; Sony Trinitron Multiscan E230) from 57 cm. The monitor showed 1280×1024 pixels (75 Hz refresh rate) and was the only source of light. A chin rest stabilized each participant's head. Participants gave their responses by pressing a key on a 4-key EGI response box with the index finger of their dominant hand.

A PC running Linux (v4.13.0), GNU Ubuntu (v16.04.4), Octave (v4.0.0) [34], and Psychophysics Toolbox (v3.0.14) [35-37]) delivered the visual stimuli and recorded behavioral responses. An iMac running EGI's NetStation 5.2 recorded EEG data.

Stimuli

We used achromatic Gabor patches (mean RGB values of 128 128 128) on an average grey background (RGB values of 128 128 128). A Gabor patch comprises a grating of a particular spatial frequency and orientation whose contrast reduces with distance from the center of the grating according to a Gaussian function [38, 39]. These stimuli are like those used by Smout et al.

Gabor patches had a contrast of .999 [Smout et al. used 1.00; we continue to give their values in brackets after ours], a phase of 0 radians—the black-to-white crossing was in the center of the patch—[not specified, but from their Figure 1, it looks the same], a spatial frequency of 2.4 cycles per degree of visual angle [2.73], and a standard deviation of the Gaussian of 3.84° of visual angle [not specified]. The visible parts of each Gabor patch had a diameter of approximately 22° of visual angle [11°, with a 0.83° central blank area]. There

bioRxiv preprint doi: https://doi.org/10.1101/2022.10.04.510779; this version posted November 24, 2022. The copyright holder for this preprint (which was not certified by peer review) is the author/funder, who has granted bioRxiv a license to display the preprint in perpetuity. It is made available under aCC-BY 4.0 International license.

were 12 possible orientations: 8°, 23°, 38°, 53°, 68°, 83°, 98°, 113°, 128°, 143°, 158°, and 173° clockwise from vertical (0°) [nine possible orientations from 0˚–160˚, in 20˚ steps].

For the participants' primary task, capitalized letters were superimposed on the center of the Gabor patch in cyan (RGB values of 0 255 255) in 30-point Courier font [a black fixation spot]. Letters occupied 0.5° (width) × 0.6° (height) with a line width of 0.06° (4 minutes) [visual angle of 0.3° diameter]. We used 25 letters of the English alphabet (all except letter 'I'). We give an illustration of this in Figure 1.

Procedure

The participants' task was to fixate on, and attend to, the continually changing random sequence of letters in the center of the monitor and to press a key with the dominant hand whenever an X appeared. Each letter occurred for 600 ms. None of the letters was immediately repeated. If the participant responded between 0.15 and 1.2 s after target onset, the response was correct. There were 383 letter changes during a block. On average, there were 15 targets (ranging from 7 to 25) per block.

Desynchronized from the letters, we presented our stimuli of interest—concentric Gabor patches—for 80 ms separated by a 280-ms inter-stimulus-interval (ISI).

We had two sorts of blocks:

1. Roving standard blocks had 634 Gabor patches of which 114 (18%) were deviants: of different orientation from the immediately preceding Gabor patches. Each deviant became the

bioRxiv preprint doi: https://doi.org/10.1101/2022.10.04.510779; this version posted November 24, 2022. The copyright holder for this preprint (which was not certified by peer review) is the author/funder, who has granted bioRxiv a license to display the preprint in perpetuity. It is made available under aCC-BY 4.0 International license.

new standard and repeated until the next deviant. For each participant and block, we organized trials into random-length sequences containing at least three standards (including the deviant of the previous sequence) and no more than 22 standards followed by a deviant. On average, five standards preceded each deviant. The deviant was randomly and equally ±15°, ±30°, or ±60° from the standard. There were 38 trials (6%) for each deviant type per block. Each block started and ended with at least three standards. The first standard in each block was one of 12 possible orientation values, chosen randomly for each participant. For example, the first few trials of one sequence might be 8°... 8°... 8°... *68*° (i.e., +60° deviant for the first sequence ...68°... 68°... 68°... 68°... *53*°... (i.e., –15° deviant for the second sequence). Figure 1(C) depicts these roving standard sequences.

2. Equiprobable blocks built from the roving standard blocks by replacing all its standard stimuli (outlined in green in Figure 1C)—except for the ones immediately preceding a deviant —with a Gabor patch whose orientation was randomly chosen among the 12 possible orientations Figure 1(D). All orientations appeared equally (8.3%) often. Deviants within oddball blocks (outlined in blue) are identical to the corresponding control stimulus (outlined in orange) in equiprobable blocks. The stimulus preceding a control stimulus (framed with two black chevrons) was identical to the stimulus preceding the deviant in the oddball block, so we

bioRxiv preprint doi: https://doi.org/10.1101/2022.10.04.510779; this version posted November 24, 2022. The copyright holder for this preprint (which was not certified by peer review) is the author/funder, who has granted bioRxiv a license to display the preprint in perpetuity. It is made available under aCC-BY 4.0 International license.

can discount the possibility that a difference in pairing (in the oddball vs. control sequences) is contributing to any deviant-related differences.

There were six oddball blocks and six equiprobable blocks. We randomized block order afresh for each participant. Each block took less than four minutes to complete. Participants were free to take breaks between blocks.

EEG recording and analysis

We recorded the electroencephalogram (EEG) using an EGI, 129-channel, dense-array HydroCel geodesic sensor net, and Net Amps 300 signal amplifier. We recorded EEG at a 500 Hz sampling rate. Impedances were below 50 kΩ as recommended by Ferree et al. [40] for the high-input impedance amplifiers. All electrodes were referenced to Cz.

We processed the EEG data offline using MATLAB 2015b (MathWorks Inc., USA), EEGLAB 14.1.1 [41], and ERPLAB 6.1.4 [42]. We re-referenced the signal of all electrodes to the common average and filtered the EEG with a low-pass 40 Hz Kaiser-windowed (beta 5.65) sinc finite impulse response (FIR) filter (order 184) followed by a high-pass 0.1 Hz Kaiser-windowed (beta 5.65) sinc FIR filter (order 9056). Epochs were 400 ms long, featuring a 50 ms pre-stimulus baseline to accommodate the short 360 ms stimulus-onset-asynchrony. We excluded epochs with amplitude changes exceeding 800 μV at any electrode

We identified electrodes with unusually high deviations in EEG activity relative to the average standard deviation pooled from all electrodes using the method described by Bigdely-Shamlo et al. [43]. A robust z-score was

bioRxiv preprint doi: https://doi.org/10.1101/2022.10.04.510779; this version posted November 24, 2022. The copyright holder for this preprint (which was not certified by peer review) is the author/funder, who has granted bioRxiv a license to display the preprint in perpetuity. It is made available under aCC-BY 4.0 International license.

calculated for each electrode by replacing the mean by the median and the standard deviation by the robust standard deviation (0.7413 times the interquartile range). We removed any electrode with a z-score exceeding 2.0 provided at least four others surrounded them for later interpolation.

We performed independent component analysis (ICA) with AMICA [44]. To improve the decomposition, we performed the analysis on raw data (excluding bad electrodes) filtered by a 1 Hz high-pass (Kaiser-windowed sinc FIR filter, order 804, beta 5.65) and 40 Hz low-pass filter, segmented into epochs, but not baseline corrected [45] as suggested by Winkler et al. [46]. We simultaneously reduced the data to 32 components.

To ensure that trials where participants moved their eyes or blinked were not included in the final analysis of the data, we created vertical and horizontal EOG channels by bipolarizing data from electrodes above and below the right eye (electrodes 8 and 126) and outer canthi of both eyes (electrodes 1 and 32), respectively (as in [47]). We identified epochs containing amplitude changes exceeding ±60 μV at these EOG channels for rejection after ICA correction.

We applied the de-mixing matrix to the 0.1−40 Hz filtered data and used SASICA [48] to identify which components exhibited low autocorrelation, low focal electrode or trial activity, high correlation with vertical or horizontal EOG, or met ADJUST criteria [49]. We assessed the remaining components using criteria described by Chaumon et al. [50], classifying components based on consistent activity time-locked to stimulus onset across all trials, on topography, or on power spectrum. We removed components identified as un-related to brain activity. We then removed epochs identified for rejection. We

bioRxiv preprint doi: https://doi.org/10.1101/2022.10.04.510779; this version posted November 24, 2022. The copyright holder for this preprint (which was not certified by peer review) is the author/funder, who has granted bioRxiv a license to display the preprint in perpetuity. It is made available under aCC-BY 4.0 International license.

performed a final artifact rejection—removing epochs containing amplitude changes exceeding ±60 μV at any electrode. Finally, using spherical splines [51], we interpolated data for removed electrodes.

For exploring deviant-related responses, we averaged ERPs for the standard, deviant, and control trials, excluding epochs immediately following a deviant or control trial. We produced difference waves by subtracting ERPs to standards and ERPs to controls from ERPs to deviants. The mean number (SD) of epochs for standards were 1994 (261), 187 (26) for 15-degree deviants, 187 (28) for 15-degree controls, 186 (28) for 30-degree deviants, 188 (30) for 30-degree controls, 188 (25) for 60-degree deviants, and 188 (27) for 60-degree controls.

For exploring repetition suppression, we averaged ERPs for standard and random stimuli at varying positions, excluding deviant and control trials. We retained standard trials immediately following deviants—in oddball sequences—and random trials immediately following controls—in equiprobable sequences. The mean number (SD) of epochs for standards were 561 (76) for 2nd sequential position (SP), 568 (73) for 3rd SP, 473 (65) for 4th SP, 350 (47) for 5th SP, 239 (35) for 6th SP, 149 (23) for 7th SP, 90 (12) for 8th SP, 120 (21) for ≥9th SP. The mean number (SD) of epochs for randoms were 563 (89) for 2nd SP, 570 (86) for 3rd SP, 478 (73) for 4th SP, 351 (54) for 5th SP, 239 (41) for 6th SP, 147 (26) for 7th SP, 90 (14) for 8th SP, and 123 (22) for ≥9th SP.

Using the EP Toolkit (v2.64; [19]), we conducted temporal principal component analysis (PCA) on the individual average ERP data for deviant and

bioRxiv preprint doi: https://doi.org/10.1101/2022.10.04.510779; this version posted November 24, 2022. The copyright holder for this preprint (which was not certified by peer review) is the author/funder, who has granted bioRxiv a license to display the preprint in perpetuity. It is made available under aCC-BY 4.0 International license.

control trials from all 129 electrodes. We used Promax orthogonal rotation ($\kappa = 3$) with a covariance relationship matrix and Kaiser weighting as recommended by Dien et al. [52]. PCA reduced the data to those components explaining most of the observed data. The component that explained the greatest amount of signal is component 1 and every component thereafter explained less of the data than the component before it. We show how much of the signal a component is responsible for by plotting the component's loading (scaled by SD) over time [53].

Using PCA, one can identify separate components in the ERP waveform and extract an alternative measure of ERP component amplitudes for inferential testing [52, 54, 55]. Each PCA component has a peak latency, a site of maximum positivity on the scalp (i.e., a component's positive pole), and a site of maximum negativity on the scalp (i.e., a component's negative pole). Plotting a topographical map of the microvolt scaled PCA data of a single component at the time of its peak latency shows the component's positive and negative pole.

A vMMN component would emerge as a component that is largest (most negative) between 150–300 ms, based on previous vMMN studies using orientation deviants (e.g., 162–170 ms in [56]; 200–250 ms in [11]; 190–220 ms in [22]). A genuine vMMN component should also yield scores that are more negative for deviants compared to controls at the component's negative pole.

We conducted Bayesian analyses of variance (ANOVAs) and paired *t*-tests to determine the likelihood of obtaining the data in addition to our

bioRxiv preprint doi: https://doi.org/10.1101/2022.10.04.510779; this version posted November 24, 2022. The copyright holder for this preprint (which was not certified by peer review) is the author/funder, who has granted bioRxiv a license to display the preprint in perpetuity. It is made available under aCC-BY 4.0 International license.

traditional ANOVAs and paired *t*-tests. We used a medium prior (with a Cauchy prior whose width was set to 0.707) for all Bayesian analyses. For interpreting our findings, a model with the largest Bayes Factor (BF_{10}) is the model that best explains the data; this is the favored model. All main effects and interactions in the favored model are, therefore, important for explaining the data. Evidence against the null is considered weak if a BF_{10} is between 1 and 3. It is positive for a BF_{10} between 3 and 20, strong for a *BF*10 between 20 and 150, and very strong given a BF_{10} greater than 150 [57].

We also performed Bayes Factor replication (BF_{r0}) tests [58] on mean amplitudes between 197 and 207 ms at each PO ROI given a prior reflecting the effect size (Cohen's $d = -0.73$) for the genuine vMMN at the PO8 in Kimura and Takeda's [22] oddball condition for 32.7° orientation deviants.

For all frequentist analyses, we applied the Greenhouse-Geisser correction where necessary ($\varepsilon<.750$). Eta squared (η^2) denotes the estimated effect size.

Author contributions

Both authors contributed to the experiment's conception, methodology, and writing – review & editing. AGM conducted formal analysis, data curation, investigation, project administration, visualization, and writing – original draft, review, and editing. ROS contributed to project administration and supervision.

bioRxiv preprint doi: https://doi.org/10.1101/2022.10.04.510779; this version posted November 24, 2022. The copyright holder for this preprint (which was not certified by peer review) is the author/funder, who has granted bioRxiv a license to display the preprint in perpetuity. It is made available under aCC-BY 4.0 International license.

Acknowledgements and Funding

We are grateful to Urte Roeber, who contributed to conception, methodology, review, and supervision. We are also grateful to the students who assisted in collecting the data for this experiment. The research was supported by an Australian Government Research Training Program Scholarship to AGM.

Conflict of interest

There are no conflicts of interest.

bioRxiv preprint doi: https://doi.org/10.1101/2022.10.04.510779; this version posted November 24, 2022. The copyright holder for this preprint (which was not certified by peer review) is the author/funder, who has granted bioRxiv a license to display the preprint in perpetuity. It is made available under aCC-BY 4.0 International license.

Supplementary Materials

1. Behavioral Results

Hit rates for oddball blocks (*M*=98.2%, *SD*=1.8%) were essentially identical for control blocks (*M*=98.2%, *SD*=2.3%), $t(20) = 0.016$, $p=.987$, $BF_{10}=0.228$. False alarm rates were similar in oddball (*M*=0.0007%, *SD*=0.0007%) and control blocks (*M*=0.0005%, *SD*=0.0005%), $t(20)=1.678$, $p=.109$, $BF_{10}=0.754$. Reaction times were essentially identical in the oddball (*M*=545 ms, *SD*=52 ms) and control blocks (545 ms, *SD*=51 ms), $t(20)=-0.025$, $p=.981$, $BF_{10}=0.228$.

2. Electrophysiological Results

2.1. vNMN

Bayesian replication confirmed that there was neither a classic nor a genuine vMMN (complete analyses in Table S1). In fact, for the classic vMMN (green traces), there was a positivity in the analyzed time window—the opposite of a vMMN. Smout et al. showed the same positivity.

2.2. Deviant-related positivity

For the deviant-related positivity (DRP), we performed a 3 × 3 × 2 repeated-measures ANOVA on P1 and N1 scores with parietal-occipital (PO) region (left vs. midline vs. right), magnitude of deviance (small vs. medium vs. large), and stimulus type (deviant vs. control) as factors.

For P1, magnitude of deviance was significant, $F(2, 40)=26.811$, $p< .001$, $\eta^2=.011$, $\varepsilon=.667$. Holm post-hoc tests showed significantly larger scores for 60° orientation change compared with 15° ($t=-7.282$, $p<.001$, $d=-0.280$) and with

bioRxiv preprint doi: https://doi.org/10.1101/2022.10.04.510779; this version posted November 24, 2022. The copyright holder for this preprint (which was not certified by peer review) is the author/funder, who has granted bioRxiv a license to display the preprint in perpetuity. It is made available under aCC-BY 4.0 International license.

30° (t=-2.974, p=.005, d=-0.114) and for 30° compared with 15° (t=-4.308, p<.001, d=-0.166). Smout et al. found similar results, albeit in their attended condition.

A ROI × stimulus interaction emerged, $F(2,40)=3.547$, $p=.038$, $\eta^2<.001$, $\varepsilon=.907$. Holm post-hoc tests showed deviants were significantly more positive than controls at LPO (t=2.882, p=.041, d=0.123), MPO (t=3.990, p=.003, d=4.293), and RPO (t=3.786, p=.010, d=3.786). The data provide very strong evidence for the favored Bayesian model including the main effects of magnitude of deviance, stimulus type, and ROI (BF_{10}=3.275e +40).

There were no significant effects or interactions for the N1 although the data provide some positive evidence for the Bayesian model including the main effect of laterality only (BF_{10}=15.961, $F(2,40)=1.261$, $p=.294$, $\eta^2=.037$, $\varepsilon=.928$).

2.3. Repetition suppression

To show the linear trends in scores for each stimulus, we show linear regressions in Figures 4 and S3 for P2 and N1 respectively. The P2 results show repetition suppression clearly, with the P2 scores declining with number of preceding standards and not with number of preceding random orientations. The N1 results are similar, except for the RPO data. Its two regression lines both show decreasing N1 scores of essentially identical slope. We must confess we have no idea why this weird result happened.

bioRxiv preprint doi: https://doi.org/10.1101/2022.10.04.510779; this version posted November 24, 2022. The copyright holder for this preprint (which was not certified by peer review) is the author/funder, who has granted bioRxiv a license to display the preprint in perpetuity. It is made available under aCC-BY 4.0 International license.

Table S1

Directed Paired (BF_{10}) and Replication (BF_{r0}) Bayesian t-tests of the Difference Wave Mean Amplitudes (µV) at Left (L), Middle (M), and Right (R) Parieto-occipital (PO) Regions Between 197 and 207 ms for Each Magnitude of Deviance (df = 20)

	Deviant vs. Standard (Classic)					**Deviant vs. Control (Genuine)**				
	µV	***t***	***p***	BF_{10}	BF_{r0}	**µV**	***t***	***p***	BF_{10}	BF_{r0}
L PO										
15° (small)	0.41	3.879	.999	0.061	0.009	0.18	1.516	.927	0.101	0.012
30° (medium)	0.55	7.701	.999	0.016	0.014	0.04	0.294	.614	0.185	0.038
60° (large)	0.71	6.871	.999	0.018	0.014	0.12	0.962	.826	0.127	0.018
M PO										
15° (small)	0.36	3.471	.998	0.064	0.008	0.16	1.060	.849	0.122	0.017
30° (medium)	0.69	4.597	.999	0.056	0.009	0.25	1.465	.921	0.103	0.012
60° (large)	0.64	4.280	.999	0.058	0.009	0.22	1.810	.957	0.092	0.011
R PO										
15° (small)	0.17	1.933	.966	0.088	0.010	0.06	0.387	.649	0.174	0.033
30° (medium)	0.48	3.464	.999	0.064	0.008	0.25	1.892	.963	0.089	0.010
60° (large)	0.54	3.617	.999	0.063	0.008	0.19	1.822	.958	0.091	0.010

Note. Time-window is the same as the time-window in which Kimura and Takeda (2015) found the largest deviant-minus-control difference at PO8 for orientation deviants of 32.7°.

bioRxiv preprint doi: https://doi.org/10.1101/2022.10.04.510779; this version posted November 24, 2022. The copyright holder for this preprint (which was not certified by peer review) is the author/funder, who has granted bioRxiv a license to display the preprint in perpetuity. It is made available under aCC-BY 4.0 International license.

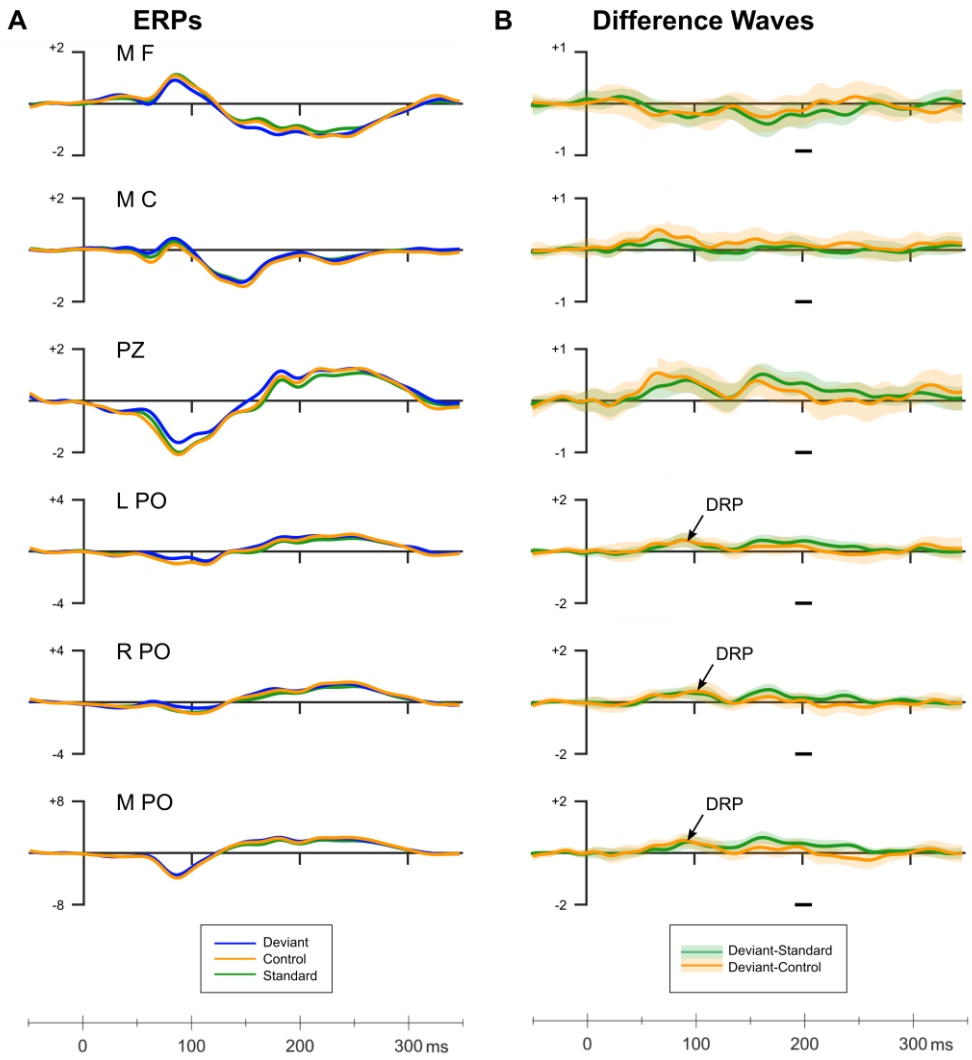

Figure S1. A. **Grand average ERPs for 15° orientation changes from various electrode clusters** around the electrodes Smout et al. reported. B. **Difference waves for classic (15-degree deviant minus standard) and genuine (15-degree deviant minus control) deviant-related activity**. The arrowed components show the only genuine deviant-related activity (DRP). Horizontal grey bars illustrate the time-window in which Kimura and Takeda (2015) found the largest deviant-minus-control difference (i.e., genuine vMMN) for 32.7° orientation deviants. Amplitudes from this time window were analyzed using Bayesian replication (results in Table S1). The lighter colors surrounding the difference waves give ± 1 standard error of the mean.

bioRxiv preprint doi: https://doi.org/10.1101/2022.10.04.510779; this version posted November 24, 2022. The copyright holder for this preprint (which was not certified by peer review) is the author/funder, who has granted bioRxiv a license to display the preprint in perpetuity. It is made available under aCC-BY 4.0 International license.

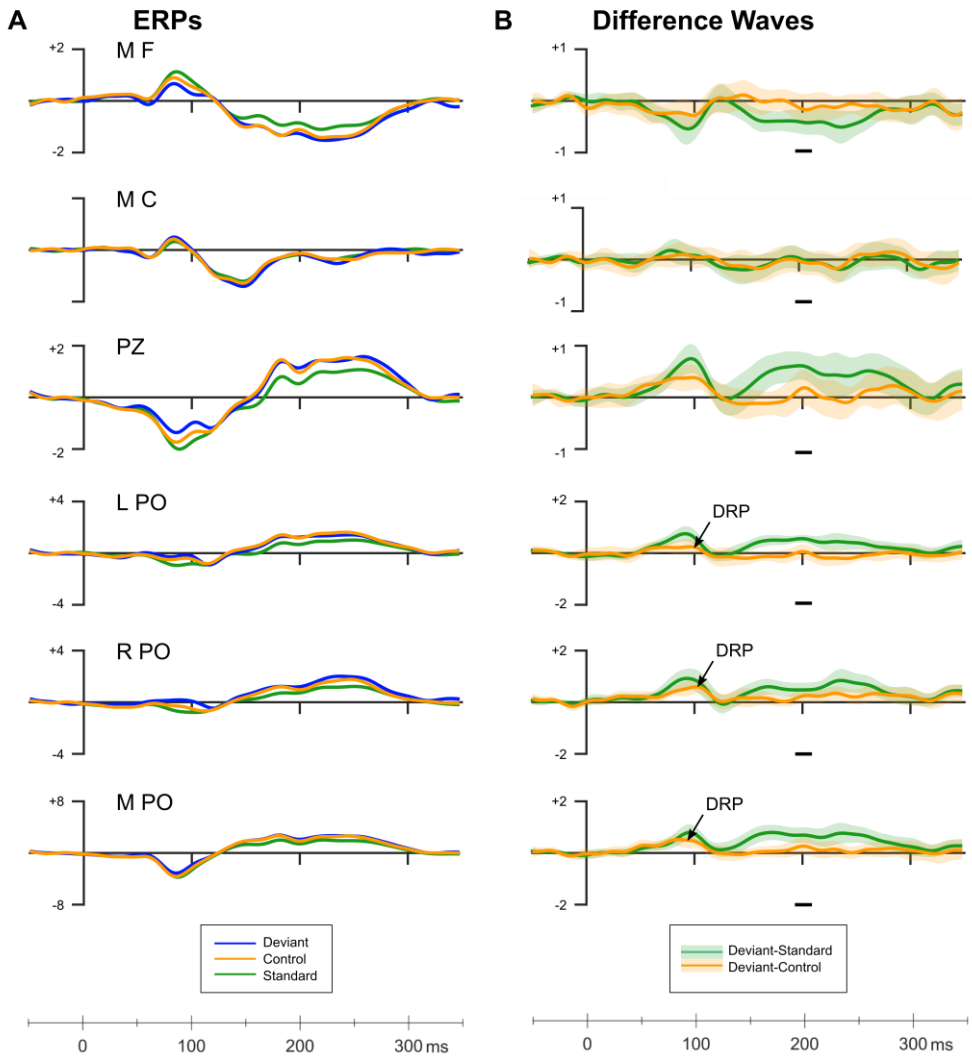

Figure S2. A. **Grand average ERPs for 30° orientation changes from various electrode clusters** around the electrodes Smout et al. reported. B. **Difference waves for classic (30-degree deviant minus standard) and genuine (30-degree deviant minus control) deviant-related activity**. The arrowed components show the only genuine deviant-related activity (DRP). Horizontal grey bars illustrate the time-window in which Kimura and Takeda (2015) found the largest deviant-minus-control difference (i.e., genuine vMMN) for 32.7° orientation deviants. Amplitudes from this time window were analyzed using Bayesian replication (results in Table S1). The lighter colors surrounding the difference waves give ± 1 standard error of the mean.

bioRxiv preprint doi: https://doi.org/10.1101/2022.10.04.510779; this version posted November 24, 2022. The copyright holder for this preprint (which was not certified by peer review) is the author/funder, who has granted bioRxiv a license to display the preprint in perpetuity. It is made available under aCC-BY 4.0 International license.

N1 Repetition Suppression Results

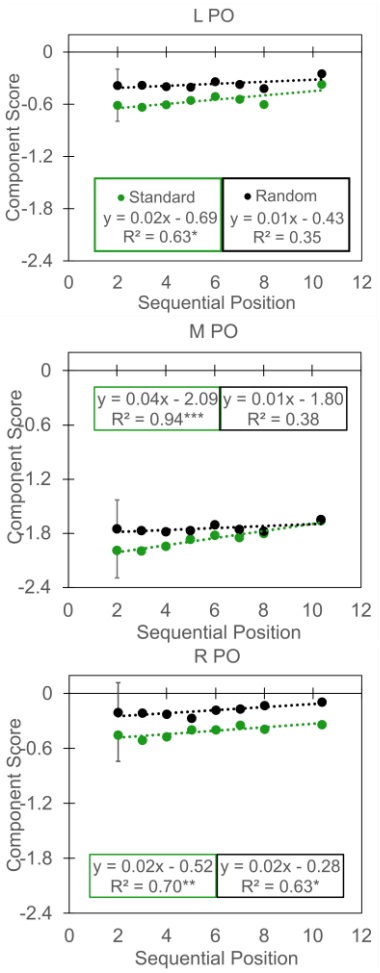

Figure S3. **N1 repetition suppression results.** N1 PCA scores are shown separately for the left (L), midline (M), and right (R) parietal-occipital (PO) regions of interest (ROI). Regression equations show the dotted lines in the data for standard and random stimuli. Asterisks denote the linear regression significance: **p*<.05, ***p*<.01, *** *p*<.001. Error bars show 1 standard error (SE) calculated as the mean SE for all sequential positions. SE bars appear only on the second sequential position. We show +1 SE for standard and –1 SE for random stimuli.

bioRxiv preprint doi: https://doi.org/10.1101/2022.10.04.510779; this version posted November 24, 2022. The copyright holder for this preprint (which was not certified by peer review) is the author/funder, who has granted bioRxiv a license to display the preprint in perpetuity. It is made available under aCC-BY 4.0 International license.

References

1. Smout CA, Tang MF, Garrido MI, Mattingley JB. Attention promotes the neural encoding of prediction errors. PLOS Biology. 2019;17(2):1-22. doi: 10.1371/journal.pbio.2006812.
2. Attneave F. Some informational aspects of visual perception. Psychological Review. 1954;61:183-93. doi: 10.1037/h0054663.
3. James W. The principles of psychology. New York: Henry Holt; 1890.
4. Srinivasan MV, Laughlin SB, Dubs A. Predictive coding: A fresh view of inhibition in the retina. Proceedings of the Royal Society Series B: Biological Sciences. 1982;216:427-59. doi: 10.1098/rspb.1982.0085.
5. Rao RPN, Ballard DH. Dynamic model of visual recognition predicts neural response properties in the visual cortex. Neural Computation. 1997;9(4):721-63. doi: 10.1162/neco.1997.9.4.721.
6. Friston K. The free-energy principle: A unified brain theory? Nature Reviews Neuroscience. 2010;11(2):127-38. Epub 2010/01/14. doi: 10.1038/nrn2787. PubMed PMID: 20068583.
7. Spratling MW. A review of predictive coding algorithms. Brain and Cognition. 2017;112:92-7. doi: 10.1016/j.bandc.2015.11.003.
8. Stefanics G, Kremláček J, Czigler I. Visual mismatch negativity: A predictive coding view. Frontiers in Human Neuroscience. 2014;8(666):1-19. doi: 10.3389/fnhum.2014.00666.
9. Paavilainen P, Alho K, Reinikainen K, Sams M, Näätänen R. Right hemisphere dominance of different mismatch negativities. Electroencephalography and Clinical Neurophysiology. 1991;78:466-79. doi: 10.1016/0013-4694(91)90064-B.
10. Bendixen A, Roeber U, Schröger E. Regularity extraction and application in dynamic auditory stimulus sequences. Journal of Cognitive Neuroscience. 2007;19:1664-77. doi: 10.1162/jocn.2007.19.10.1664.
11. Kimura M, Katayama JI, Ohira H, Schröger E. Visual mismatch negativity: New evidence from the equiprobable paradigm. Psychophysiology. 2009;46:402-9. doi: 10.1111/j.1469-8986.2008.00767.x.
12. Hubel DH, Wiesel TN. Receptive fields and functional architecture of monkey striate cortex. Journal of Physiology. 1968;195:215-43.
13. Auksztulewicz R, Friston K. Attentional enhancement of auditory mismatch responses: A DCM/MEG study. Cerebral Cortex. 2015;25(11):4273-83. doi: 10.1093/cercor/bhu323.
14. Schwartz EL. Computational anatomy and functional architecture of striate cortex: A spatial mapping approach to perceptual coding. Vision Research. 1980;20(8):645-69. doi: https://doi.org/10.1016/0042-6989(80)90090-5.
15. Male AG, O'Shea RP, Schröger, E.,, Müller D, Roeber U, Widmann A. The quest for the genuine visual mismatch negativity (vMMN): Event-related potential indications of deviance detection for low-level visual features. Psychophysiology. 2020;1(1):1–10. doi: https://doi.org/10.1111/psyp.13576.

bioRxiv preprint doi: https://doi.org/10.1101/2022.10.04.510779; this version posted November 24, 2022. The copyright holder for this preprint (which was not certified by peer review) is the author/funder, who has granted bioRxiv a license to display the preprint in perpetuity. It is made available under aCC-BY 4.0 International license.

16. Scrivener CL, Reader AT. Variability of EEG electrode positions and their underlying brain regions: Visualizing gel artifacts from a simultaneous EEG-fMRI dataset. Brain and Behavior. 2022;12(2):e2476. doi: 10.1002/brb3.2476.
17. Grill-Spector K, Henson R, Martin A. Repetition and the brain: Neural models of stimulus-specific effects. Trends in Cognitive Sciences. 2006;10:14-23. Epub 2005/12/03. doi: 10.1016/j.tics.2005.11.006. PubMed PMID: 16321563.
18. Tang MF, Smout CA, Arabzadeh E, Mattingley JB. Prediction error and repetition suppression have distinct effects on neural representations of visual information. eLife. 2018;7(e33123):1-21. doi: 10.7554/eLife.33123.
19. Dien J, Khoe W, Mangun GR. Evaluation of PCA and ICA of simulated ERPs: Promax vs. infomax rotations. Human Brain Mapping. 2007;28(8):742-63. doi: https://doi.org/10.1002/hbm.20304.
20. File D, File B, Bodnár F, Sulykos I, Kecskés-Kovács K, Czigler I. Visual mismatch negativity (vMMN) for low- and high-level deviances: A control study. Attention, Perception, & Psychophysics. 2017;79(7):2153-70. doi: 10.3758/s13414-017-1373-y.
21. Sulykos I, Kecskés-Kovács K, Czigler I. Mismatch Negativity Does Not Show Evidence of Memory Reactivation in the Visual Modality. Journal of Psychophysiology. 2013;27(1):1-6. doi: 10.1027/0269-8803/a000085.
22. Kimura M, Takeda Y. Automatic prediction regarding the next state of a visual object: Electrophysiological indicators of prediction match and mismatch. Brain Research. 2015:31-44. doi: doi:10.1016/j.brainres.2015.01.013. PubMed PMID: 25598206.
23. Astikainen P, Ruusuvirta T, Wikgren J, Korhonen T. The human brain processes visual changes that are not cued by attended auditory stimulation. Neuroscience Letters. 2004;368(2):231-4. doi: 10.1016/j.neulet.2004.07.025. PubMed PMID: 15351455.
24. Kimura M, Takeda Y. Task difficulty affects the predictive process indexed by visual mismatch negativity. Frontiers in Human Neuroscience. 2013;7(267):1-13. doi: 10.3389/fnhum.2013.00267.
25. Burbeck CA, Regan D. Independence of orientation and size in spatial discriminations. J Opt Soc Am. 1983;73(12):1691-4. Epub 1983/12/01. doi: 10.1364/josa.73.001691. PubMed PMID: 6663372.
26. Czigler I, Balázs L, Winkler I. Memory-based detection of task-irrelevant visual changes. Psychophysiology. 2002;39(6):869-73. doi: 10.1111/1469-8986.3960869.
27. Schmitt C, Klingenhoefer S, Bremmer F. Preattentive and predictive processing of visual motion. Scientific Reports. 2018;8(12399):1-12. doi: 10.1038/s41598-018-30832-9.
28. Berti S, Schröger E. A comparison of auditory and visual distraction effects: behavioral and event-related indices. Cognitive Brain Research. 2001;10(3):265-73. doi: 10.1016/S0926-6410(00)00044-6.
29. Chen Y, Huang X, Luo Y, Peng C, Liu C. Differences in the neural basis of automatic auditory and visual time perception: ERP evidence from an

bioRxiv preprint doi: https://doi.org/10.1101/2022.10.04.510779; this version posted November 24, 2022. The copyright holder for this preprint (which was not certified by peer review) is the author/funder, who has granted bioRxiv a license to display the preprint in perpetuity. It is made available under aCC-BY 4.0 International license.

across-modal delayed response oddball task. Brain Research. 2010;1325:100-11. doi: https://doi.org/10.1016/j.brainres.2010.02.040.
30. Kimura M, Katayama J, Murohashi H. Independent processing of visual stimulus changes in ventral and dorsal stream features indexed by an early positive difference in event-related brain potentials. International Journal of Psychophysiology. 2006;59(2):141-50. doi: https://doi.org/10.1016/j.ijpsycho.2005.03.023.
31. Fu S, Fan S, Chen L. Event-related potentials reveal involuntary processing of orientation changes in the visual modality. Psychophysiology. 2003;40(5):770-5. doi: 10.1111/1469-8986.00077.
32. Müller D, Roeber U, Winkler I, Trujillo-Barreto N, Czigler I, Schröger E. Impact of lower- vs. upper-hemifield presentation on automatic colour-deviance detection: A visual mismatch negativity study. Brain Research. 2012;1472:89-98. doi: https://doi.org/10.1016/j.brainres.2012.07.016.
33. Sysoeva OV, Lange EB, Sorokin AB, Campbell T. From pre-attentive processes to durable representation: An ERP index of visual distraction. International Journal of Psychophysiology. 2015;95(3):310-21. doi: 10.1016/j.ijpsycho.2014.12.007.
34. Eaton JW, Bateman D, Hauberg S, Wehbring R. GNU Octave version 3.8.1 manual: A high-level interactive language for numerical computations.: CreateSpace Independent Publishing Platform; 2014.
35. Brainard DH. The Psychophysics Toolbox. Spatial Vision. 1997;10(4):433-6.
36. Kleiner M, Brainard D, Pelli D, Ingling A, Murray R, Broussard C, editors. What's new in psychtoolbox-3. Proceedings of European Conference of Visual Perception; 2007: Perception.
37. Pelli DG. The VideoToolbox software for visual psychophysics: Transforming numbers into movies. Spatial Vision. 1997;10(4):437-42.
38. Bruce V, Green PR, Georgeson MA. Visual perception: physiology, psychology, & ecology. 4th ed. Hove;New York;: Psychology Press; 2003.
39. Fredericksen RE, Bex PJ, Verstraten FAJ. How big is a Gabor patch, and why should we care? errata. Journal of the Optical Society of America A: Optics and Image Science, and Vision. 1998;15(7):1. doi: 10.1364/JOSAA.15.001959.
40. Ferree TC, Luu P, Russell GS, Tucker DM. Scalp electrode impedance, infection risk, and EEG data quality. Clinical Neurophysiology. 2001;112:538–44. doi: https://dx.doi.org/10.1016/S1388-2457(00)00533-2.
41. Delorme A, Makeig S. EEGLAB: an open source toolbox for analysis of single-trial EEG dynamics including independent component analysis. Journal of Neuroscience Methods. 2004;134(1):9-21. doi: https://doi.org/10.1016/j.jneumeth.2003.10.009.
42. Lopez-Calderon J, Luck SJ. ERPLAB: an open-source toolbox for the analysis of event-related potentials. Frontiers in Human Neuroscience. 2014;8(213). doi: 10.3389/fnhum.2014.00213.
43. Bigdely-Shamlo N, Mullen T, Kothe C, Su K, Robbins KA. The PREP pipeline: Standardized preprocessing for large-scale EEG analysis.

bioRxiv preprint doi: https://doi.org/10.1101/2022.10.04.510779; this version posted November 24, 2022. The copyright holder for this preprint (which was not certified by peer review) is the author/funder, who has granted bioRxiv a license to display the preprint in perpetuity. It is made available under aCC-BY 4.0 International license.

Frontiers in Neuroinformatics. 2015;9(16):1-20. doi: 10.3389/fninf.2015.00016. PubMed PMID: 26150785.
44. Palmer J, Kreutz-Delgado K, Makeig S. AMICA: An Adaptive Mixture of Independent Component Analyzers with Shared Components. http://dsp.ucsd.edu/~kreutz/Publications/palmer2011AMICA.pdf. San Diego: 2011.

45. Groppe DM, Makeig S, Kutas M. Identifying reliable independent components via split-half comparisons. NeuroImage. 2009;45(4):1199-211. Epub 12/31. doi: 10.1016/j.neuroimage.2008.12.038. PubMed PMID: 19162199.
46. Winkler I, Debener S, Müller KR, Tangermann M. On the influence of high-pass filtering on ICA-based artifact reduction in EEG-ERP. Annu Int Conf IEEE Eng Med Biol Soc. 2015;2015:4101-5. Epub 2016/01/07. doi: 10.1109/embc.2015.7319296. PubMed PMID: 26737196.
47. Maekawa T, Katsuki S, Kishimoto J, Onitsuka T, Ogata K, Yamasaki T, et al. Altered visual information processing systems in bipolar disorder: evidence from visual MMN and P3. Front Hum Neurosci. 2013;7:403. Epub 2013/07/31. doi: 10.3389/fnhum.2013.00403. PubMed PMID: 23898256; PubMed Central PMCID: PMCPMC3724050.
48. Makeig S, Bell AJ, Jung TP, Sejnowski TJ. Independent component analysis of electroencephalographic data. In: Touretzky D, Mozer M, Hasselmo M, editors. Advances in Neural Information Processing Systems. MIT Press: Cambridge; 1996.
49. Mognon A, Jovicich J, Bruzzone L, Buiatti M. ADJUST: An automatic EEG artifact detector based on the joint use of spatial and temporal features. Psychophysiology. 2011;48(2):229-40. doi: 10.1111/j.1469-8986.2010.01061.x.
50. Chaumon M, Bishop DVM, Busch NA. A practical guide to the selection of independent components of the electroencephalogram for artifact correction. Journal of Neuroscience Methods. 2015;250(Supplement C):47-63. doi: https://doi.org/10.1016/j.jneumeth.2015.02.025.
51. Perrin F, Pernier J, Bertnard O, Giard MH, Echallier JF. Mapping of scalp potentials by surface spline interpolation. Electroencephalography and Clinical Neurophysiology. 1987;66(1):75-81. doi: 10.1016/0013-4694(87)90141-6.
52. Dien J, Frishkoff G. Introduction to Principal Components Analysis of Event-Related Potentials. In: Handy T, editor. Event Related Potentials: A Methods Handbook Cambridge, Mass: MIT Press; 2005.
53. Dien J. Applying principal components analysis to event-related potentials: a tutorial. Dev Neuropsychol. 2012;37(6):497-517. Epub 2012/08/15. doi: 10.1080/87565641.2012.697503. PubMed PMID: 22889342.
54. Carretié L, Tapia M, Mercado F, Albert J, López-Martín S, de la Serna JM. Voltage-based versus factor score-based source localization analyses of electrophysiological brain activity: A comparison. Brain Topography. 2004;17(2):109-15. doi: 10.1007/s10548-004-1008-1.

bioRxiv preprint doi: https://doi.org/10.1101/2022.10.04.510779; this version posted November 24, 2022. The copyright holder for this preprint (which was not certified by peer review) is the author/funder, who has granted bioRxiv a license to display the preprint in perpetuity. It is made available under aCC-BY 4.0 International license.

55. Dien J. The ERP PCA Toolkit: An open source program for advanced statistical analysis of event-related potential data. Journal of Neuroscience Methods. 2010;187(1):138-45. doi: https://doi.org/10.1016/j.jneumeth.2009.12.009.
56. Czigler I, Sulykos I. Visual mismatch negativity to irrelevant changes is sensitive to task-relevant changes. Neuropsychologia. 2010;48(5):1277-82. doi: 10.1016/j.neuropsychologia.2009.12.029. PubMed PMID: 20036268.
57. Raftery AE. Bayesian model selection in social research. In: Marsden PV, editor. Sociological methodology. Cambridge, MA: Blackwell; 1995. p. 111–96.
58. Verhagen J, Wagenmakers EJ. Bayesian tests to quantify the result of a replication attempt. Journal of Experimental Psychology General. 2014;143(4):1457-75. doi: 10.1037/a0036731.